





## RESEARCH ARTICLE OPEN ACCESS

# Development and Characterization of the NISTCHO Reference Cell Line

Hussain Dahodwala<sup>1</sup> | Irfan Hodzic<sup>2</sup> | Alexei Slesarev<sup>3</sup> | Benjamin Cutak<sup>4</sup> | Alexander Kuzin<sup>3</sup> | Rahul Lal<sup>5</sup> | Jiajian Liu<sup>6</sup> | James Mahon<sup>2</sup> | Rajagopalan Lakshmi Narasimhan<sup>5</sup> | Jaya Onuska<sup>3</sup> | James Ravellette<sup>2</sup> | Kelsey Reger<sup>2</sup> | Sadie Sakurada<sup>2</sup> | Floy Stewart<sup>2</sup> | Trissa Borgschulte<sup>2</sup>  | Colette Cote<sup>3</sup> | Kelvin H. Lee<sup>1</sup>  | William B. O'Dell<sup>7,8</sup> | Zvi Kelman<sup>7,8</sup>  | Britta A. Anderson<sup>2</sup> 

<sup>1</sup>National Institute for Innovation in Manufacturing Biopharmaceuticals, University of Delaware, Newark, Delaware, USA | <sup>2</sup>Process Solutions, MilliporeSigma, St. Louis, Missouri, USA | <sup>3</sup>Life Science Services, MilliporeSigma, Rockville, Maryland, USA | <sup>4</sup>Central Analytics, MilliporeSigma, St. Louis, Missouri, USA |

<sup>5</sup>Bioinformatics, IT R&D Applications, Sigma-Aldrich Chemicals Pvt. Ltd., A subsidiary of Merck KGaA, Darmstadt, Germany, Bangalore, India |

<sup>6</sup>Bioinformatics, Analytics Center of Excellence, MilliporeSigma, St. Louis, Missouri, USA | <sup>7</sup>Biomolecular Measurement Division, National Institute of Standards and Technology, Gaithersburg, Maryland, USA | <sup>8</sup>Biomolecular Labeling Laboratory, Institute for Bioscience and Biotechnology Research, University of Maryland, Rockville, Maryland, USA

**Correspondence:** Zvi Kelman ([zkelman@umd.edu](mailto:zkelman@umd.edu); [zvi.kelman@nist.gov](mailto:zvi.kelman@nist.gov)) | Britta A. Anderson ([britta.anderson@milliporesigma.com](mailto:britta.anderson@milliporesigma.com))

**Received:** 18 October 2024 | **Revised:** 21 February 2025 | **Accepted:** 18 March 2025

**Funding:** H.D. and K.H.L. would like to acknowledge support from the Department of Commerce NIST through 70NANB17H002.

**Keywords:** cell culture | cell line development | monoclonal antibody | NISTCHO | reference cell line | transgene integration sites

## ABSTRACT

Well-characterized reference materials enable successful collaborations within the scientific community by establishing common reagents for benchmarking studies and reducing the barriers to sharing materials and information. Here, we report the development of NISTCHO, a recombinant Chinese hamster ovary cell line expressing a nonoriginator version of the NISTmAb IgG1. We evaluated candidate clonal cell lines in a fed-batch cell culture model to assess growth and productivity of the cell lines and protein quality attributes of the recombinant IgG produced, which demonstrated suitability of multiple candidates. Selection of a preferred candidate was accomplished through sequencing-based analysis of the transgene integration sites, and a base-pair resolution map of the transgene integration site was developed and verified using PCR-based methods. Lastly, a validation study performed by an independent laboratory confirmed the robustness of the preferred candidate, which has been selected for further development as the NISTCHO reference cell line. Together, these results describe the origin of this new reference material and will serve as the foundation for future interlaboratory studies using the NISTCHO cell line.

## 1 | Introduction

Comparison of methods and results between scientists, laboratories, and organizations is a fundamental principle in scientific discourse. Well-characterized reference materials enable metro-

logical traceability [1], or the ability to relate a measurement to an accepted standard, by providing investigators with experimental reagents with known properties. The US-based National Institute of Standards and Technology (NIST) develops, characterizes, and distributes Standard Reference Materials to support the

Hussain Dahodwala, Irfan Hodzic, and Alexei Slesarev contributed equally to this study and are considered joint first authors.

Certain equipment, instruments, software, or materials are identified in this paper in order to specify the experimental procedure adequately. Such identification is not intended to imply recommendation or endorsement of any product or service by NIST, nor is it intended to imply that the materials or equipment identified are necessarily the best available for the purpose.

This is an open access article under the terms of the [Creative Commons Attribution-NonCommercial-NoDerivs](https://creativecommons.org/licenses/by-nc-nd/4.0/) License, which permits use and distribution in any medium, provided the original work is properly cited, the use is non-commercial and no modifications or adaptations are made.

© 2025 Sigma-Aldrich, LLC and The Author(s). *Biotechnology Journal* published by Wiley-VCH GmbH. This article has been contributed to by U.S. Government employees and their work is in the public domain in the USA.

development of new methods and definition of experimental best practices. For the biopharmaceutical industry, the IgG1 $\kappa$  monoclonal antibody NIST Monoclonal Antibody Reference Material 8671 NISTmAb, commonly known as RM 8671 NISTmAb or simply NISTmAb [2], has rapidly become a ubiquitous reagent to assess instrument performance and benchmark biopharmaceutical analytical methods.

The availability of similarly well-characterized reference cell lines for the biopharmaceutical community remains a significant challenge. Standards for authentication of cell lines have been developed to improve reproducibility [3, 4], but challenges continue to arise from differences in handling practices and cell culture reagents. Access to reference cell lines with metrological traceability along with transparent cell culture protocols and performance standards will further improve reproducibility and enable more rigorous definition of industry best practices. To meet this need for the broader scientific community, here we report the development and initial characterization of a biopharmaceutically relevant cell line that is the first of its kind at NIST. This cell line, named NISTCHO, is a recombinant Chinese hamster ovary (CHO) cell line developed in the commercially available CHOZN GS<sup>-/-</sup> platform and produces a nonoriginator version of the NISTmAb IgG1 (here, this product will be referred to as cNISTmAb-MPSG [5]; expanded definitions relating to product nomenclature can be found in the Materials and Methods section).

## 2 | Results

### 2.1 | Candidate NISTCHO Cell Lines Demonstrate Diverse Growth and Productivity Phenotypes

Candidate clonal cell lines expressing cNISTmAb-MPSG were generated through the cell line development workflow summarized in Figure 1A and further elaborated upon in Supplemental File 1 and Figure S1. These candidate cell lines produce a recombinant IgG that is expected to have the same primary amino acid sequence as RM 8671 NISTmAb. For details regarding the criteria used in the clone selection process, please refer to the Discussion and Figure 5. The growth and productivity of six clonal cell lines were assessed in a fed-batch production assay in a spin tube cell culture model using EX-CELL Advanced Fed-Batch basal medium and EX-CELL Advanced CHO Feed 1 (Figures 1B–D), where a range of growth and productivity phenotypes were observed. Clones 2 and 6 showed the highest cell-specific productivities (29.3–39.6 pg/cell/day) but reached the lowest peak viable cell densities ( $8.2 - 9.9 \times 10^6$  cells/mL). While the viability of clone 6 remained above 95% through day 19 of the assay, the viability of clone 2 dropped below 90% on assay day 11 and continued a slow decline until assay day 19, when it reached the 70% viability threshold. Clones 15, 21, and 31 performed very similarly to one another despite originating from different parental minipools, and these clones showed moderately high peak viable cell densities ( $15.6 - 19.4 \times 10^6$  cells/mL) and modest cell-specific productivities (10.2–14.7 pg/cell/day). Clones 15 and 21 demonstrated viability greater than 98% and 90% through day 21 of the assay. Clone 31 showed a distinct viability profile compared to the other cell lines, declining below 90% viability at assay day 11 and below 70% viability on assay

day 15. Clone 13 showed the highest peak viable cell density of  $27.8 - 36.2 \times 10^6$  cells/mL (spanning duplicate samples) but also the lowest cell-specific productivity, ranging from 7.8 to 15.4 pg/cell/day throughout the duration of the experiment. Clone 13 demonstrated viability greater than 90% through assay day 19.

### 2.2 | Candidate Cell Lines Improve Volumetric Productivity and Maintain Expression Stability Using an Alternative Feed Strategy

Optimization of cell culture medium and feeding regimens are common strategies used to improve cell culture performance [6, 7]. Therefore, we evaluated these six cell lines in a fed-batch productivity assay in a spin tube cell culture model using an alternative feeding strategy previously described to improve volumetric productivity and culture duration in the CHOZN GS<sup>-/-</sup> platform [8] (refer to Materials and Methods for details). When this protocol was used, all six clonal cell lines showed an increase in peak volumetric titer, but the mechanism by which this increase was achieved varied (Figure 1E–G). For clone 2, the productivity increase from 2.0 to 5.9 g/L was driven by increased culture longevity, with both culture replicates maintaining viability > 70% for an additional 8 days. While clone 6 maintained > 70% viability for 21 days in the original conditions, higher viability was also observed beyond day 11 in the alternative feeding strategy, increasing the volumetric titer from 4.6 to 6.2 g/L. In addition, a modest increase in cell-specific productivity was observed for this clone, ranging from 44.3 to 49.9 pg/cell/day between days 11 and 15. For clones 13, 15, and 21, increases in IgG titer were driven by increases in viable cell density in the terminal days of the assay and a slight increase in cell-specific productivity. A modest increase in volumetric productivity was observed for clones 13 (from 3.1 g/L previously to 4.6 g/L) and 15 (from 2.7 g/L previously to 3.4 g/L), but for clone 21 a larger increase from 3.1 g/L to 6.1 g/L was observed due to these combined factors. The increase from 1.7 to 2.6 g/L for Clone 31 (Figure 1H) was driven by a 10% increase in peak viable cell density with the blended feed. Comparisons of peak volumetric titer between assay conditions are found in Figure 1H.

Maintenance of protein expression through extended time in culture is an essential characteristic for biotherapeutic-expressing cell lines, and cell line instability can be caused by a variety of different mechanisms [9]. To assess the stability of recombinant protein expression of the candidate cell lines, cell lines were passaged twice weekly for 10 weeks (20 passages), representing population doubling levels of 60 (clone 2), 58 (clone 6), 64 (clone 13), 62 (clones 15 and 31), and 65 (clone 21) compared to the research cell bank (RCB) established for each clone (Figure 1I). Recombinant protein titers were evaluated for cultures derived from the RCB and from the P20 banks, using both feeding regimens that were previously evaluated. Details of this study are described in Supplemental File 1 (Figure S2) and are summarized in Figure 1I, which reports the P20 volumetric titer as a percentage of the titer derived from the RCB for each cell line evaluated using the designated feeding strategy. Apart from clone 21 under the standard feeding regimen, all clonal cell lines met or exceeded 70% of the titer of the culture derived from the RCB after reaching the defined population doubling level, a reported mark indicating acceptable stability of protein expression [9]. Interestingly,

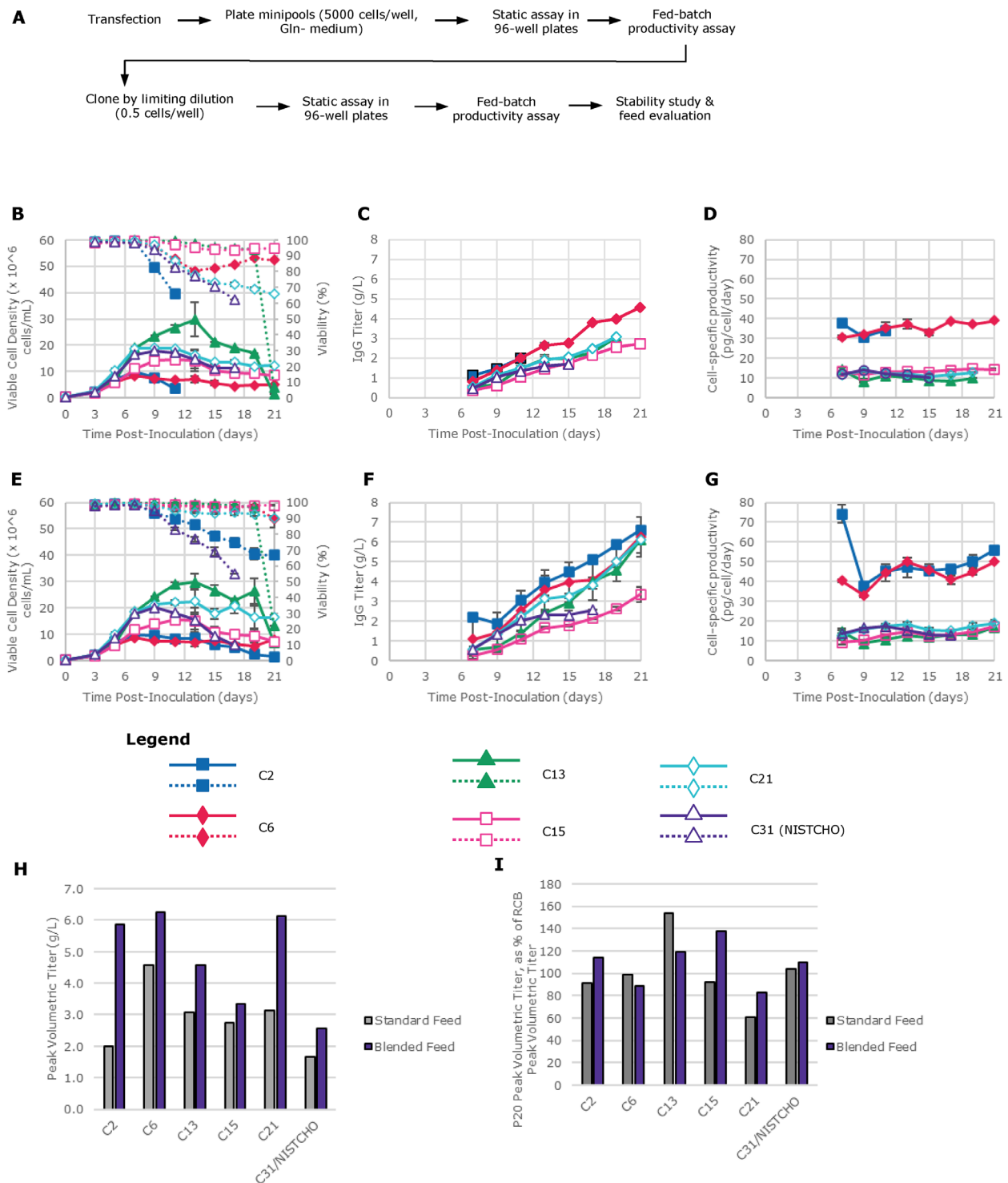


**FIGURE 1** | All candidate clonal cell lines meet initial criteria for growth and productivity assessments in spin tube cell culture models. (A) Cell line development workflow identifying key steps in selection, single cell cloning, and growth, and productivity evaluation. (B) Growth of candidate clonal cell lines in standard fed-batch process measured by viable cell density (solid lines) and viability (dotted lines, secondary axis). (C) Titer of candidate clonal cell lines in standard fed-batch process. (D) Cell-specific productivity of candidate clonal cell lines in standard fed-batch process. (E) Growth of candidate clonal cell lines in fed-batch process using alternative feed strategy measured by viable cell density (solid lines) and viability (dotted lines, secondary axis). (F) Titer of candidate clonal cell lines in fed-batch process using alternative feed strategy. (G) Cell-specific productivity of candidate clonal cell lines in fed-batch process using alternative feed strategy. In panels (B)–(G), clones are represented as follows: clone 2, solid blue squares; clone 6, solid red diamonds; clone 13, solid green triangles; clone 15, open pink squares; clone 21, open aqua diamonds; clone 31 (NISTCHO), open purple triangles. Data are reported as the average of duplicate samples with error bars representing one standard deviation. Absent error bars indicate that one of two duplicate samples was terminated due to low viability. (H) Peak volumetric titer, summarized from panels (C) and (F); data are reported as the average of duplicate samples. (I) Assessment of expression stability based on peak volumetric titer, reported as P20 as a percentage of RCB. RCB, research cell bank.

two cell line and feed combinations demonstrated significant increases (> 30%) in volumetric titer at passage 20. For clone 13 using the standard feed strategy, a faster decline in culture viability and lower viable cell density was observed in the P20 cultures (Figure S2A,2B), which could result in higher volumetric titers due to cell lysis. For clone 15 under the alternative feed strategy, a higher viable cell density was observed in the P20 cultures (Figure S2D).

### 2.3 | Transgene Integration Sites Can Be Used for Unambiguous Identification of NISTCHO

The genomes of recombinant cell lines contain unique combinations of targeted and spontaneous genetic changes, which can be exploited to support cell line authentication [3, 4, 10]. In addition to short tandem repeat profiling, the unique genomic structures that arise from random integration of an expression vector into the host cell genome can also be leveraged to support the authentication of NISTCHO and importantly, its distinction from other recombinant CHO cell lines expressing cNISTmAb-MPSG. To assess the transgene integration site in these clonal cell lines and evaluate methods for cell line authentication, we first leveraged the RGEN method [11, 12] to determine the location and structure of the transgenes in the same six candidate cell lines. Here, guide RNAs designed throughout the expression vector were used to enrich for transgene integration sites, regardless of the genomic location, copy number, or structure of the transgene integration site (see Supplemental File 1 and Figure S3 for an expanded discussion of the method and results).

The six candidate clonal cell lines demonstrated a wide range of integration site profiles (Figure 2A; Supplemental File 1 and Figures S4–S9), revealing important insights that were highly impactful in the selection of a reference cell line. Clone 13 possessed the longest vector integration site, comprised of three full-length and seven truncated vector copies arranged in a head-to-tail orientation. Clones 2 and 6, which were derived from the same parental minipool, possess identical transgene structures comprised of four complete vector copies and a fifth truncated copy arranged as an inverted repeat. Clone 21 demonstrated the most complex integration structure, consisting of eight vector copies, all of which were truncated to some extent. Interestingly, the repetitive genomic flanking sequences suggested integration into a microsatellite, repetitive element, or telomeric region. Clone 15 is the sole cell line with a single vector copy integrated in a single locus. While the 5' and 3' flanking regions of the integration site align to different scaffolds in most available CHO genomes, when evaluated against the available PICRH CHO genome [13], the alignment of the flanking sequences indicate a possible > 1 Mb chromosomal rearrangement at the 5' end of the transgene. Lastly, clone 31 demonstrated an intact integrated vector lacking vector–vector junctions, with clearly defined breakpoints on both the 5' and 3' ends of the transgene. Interestingly, the inferred copy number of the expression vector based on sequence coverage was approximately 3, suggesting a more complex genomic duplication and rearrangement may have occurred.

To confirm the expected integration site pattern in Clone 31 and to further assess the transgene vector integrity and sequence, we

performed whole genome, paired-end Illumina sequencing on genomic DNA isolated from clone 31 and applied the analytical approach described in Supplemental File 1 (Figure S10). In agreement with the long-read approach previously described, the short read sequencing identified the chromosomal break point for integration of the transgene at the location chr3: 4977278–4977293 (Figure 2B; Supplemental File 1, Figure S10, Table S1). Furthermore, it also established that the integrated transgene is free of any fixed point mutations that would have arisen prior to establishment of monoclonality. An expanded discussion of these results is presented in Supplemental File 1.

Finally, we assessed the transgene and integration site using PCR to assess the utility of a more tractable and accessible method. Using droplet digital PCR, we established that the transgene is present within clone 31 as 3 copies (Figure 2C), normalized to the *Slc35a1* gene which is present in only a single copy in the hypodiploid CHO genome [14, 15]. To further elucidate the relationship between the calculated vector copy number data and the sequencing results, we assessed the transgene-chromosome junctions on both the 5' and 3' ends of the transgene. Amplification using these primer sets generates products with the expected size, further confirming the previously identified transgene integration site (Figure 2D). However, when primer sets spanning the transgene-chromosome junctions are used with droplet digital PCR to assess the copy number of these junctions, comparison of the junction amplicon to either a single-copy gene (*Slc35a1*) or a gene expected to be present in three copies in the CHOZN GS genome [14] (*Fbxw2*) demonstrated amplicon ratios consistent with three independently integrated copies of the transgene (Figure 2E). While these PCR-based methods are robust and more accessible than sequencing-based methods, they cannot establish whether this transgene integration structure arose from aneuploidy (duplication of the entire chromosome containing the transgene) or duplication of a larger part of a chromosome.

### 2.4 | cNISTmAb-MPSG From NISTCHO Maintains Biopharmaceutically-Relevant Product Quality Attributes

Posttranslational modifications of protein-based therapeutics have significant impacts on therapeutic safety and efficacy [16, 17]. Some quality attributes such as N-linked glycosylation patterns, charge variant profiles, or levels of aggregated or fragmented proteins, are routinely assessed during cell line development to ensure selection of an optimal cell line for manufacturing. Therefore, we evaluated several protein quality attributes from cNISTmAb-MPSG samples collected at assay day 14 in the spin tube cell culture production assay described in Figure 1E–G. The cNISTmAb-MPSG product quality attributes from clone 31 are described in Figure 3, while chromatograms and attributes for cNISTmAb-MPSG produced by clones 2, 6, 13, 15, and 21 are reported in Supplemental File 1 (Figures S11–S13).

We first evaluated the high-molecular weight aggregate and low-molecular weight fragment profiles of the material produced by each clonal cell line by size exclusion chromatography-HPLC (SEC-HPLC). The profile of the cNISTmAb-MPSG produced by clone 31 is indicative of a monomeric protein complex, in this

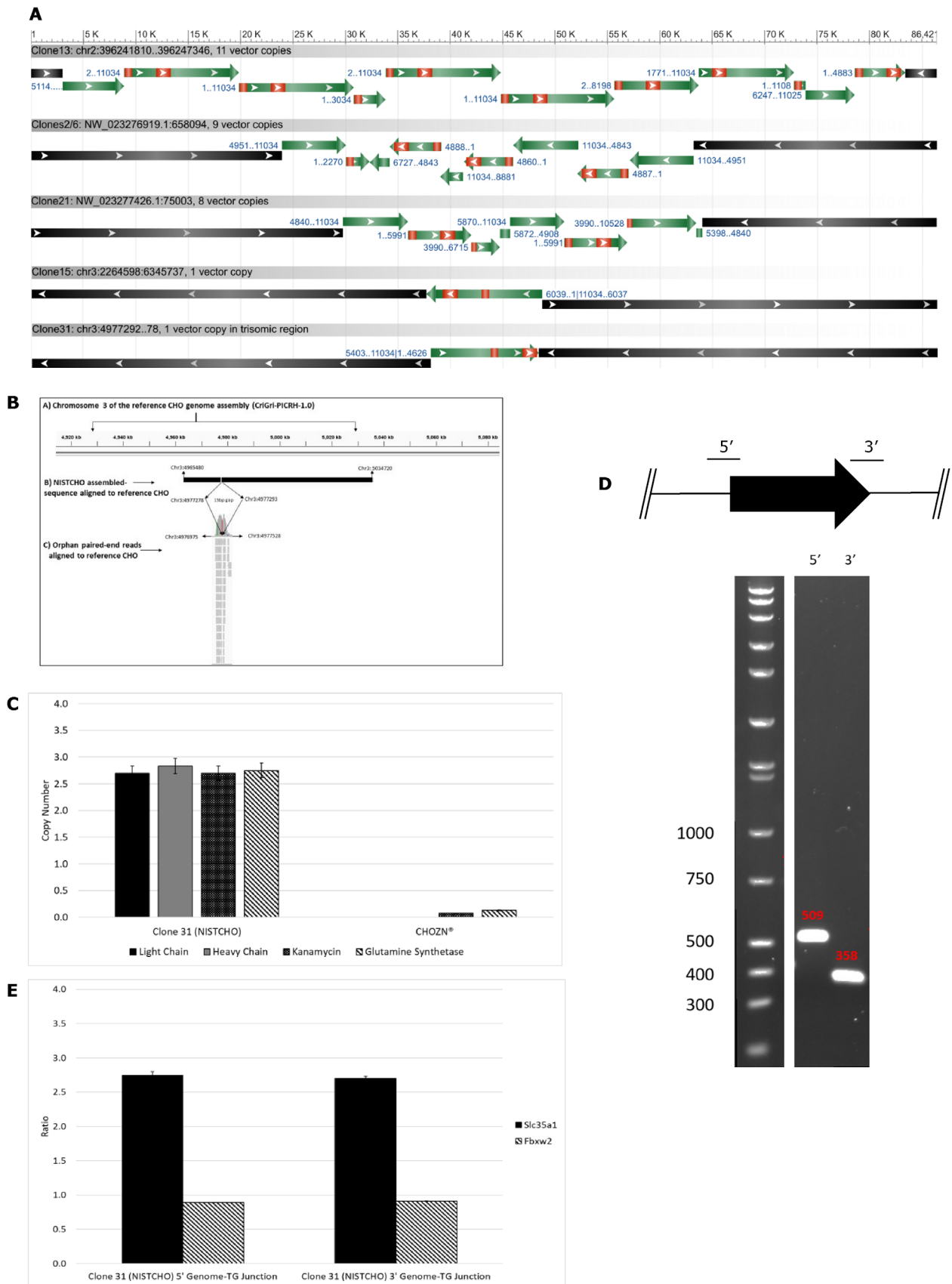


**FIGURE 2** | Transgene integration profiles identify a preferred candidate for a reference cell line. (A) Map of the vector integration sites observed in the tested NIST CHO clones through long read sequencing (Nanopore). The vector backbones and transgenes are color-coded (green and red, respectively), and their sizes are depicted to scale. The identified fusion breakpoints are also indicated. Clones 2 and 6 exhibit identical integration patterns, while Clone 31 displays a single vector integration in chromosome 3. (B) Scaffold-wide view of transgene integration site identified by whole genome sequencing. At the top, label (A) represents the chromosome 3 scaffold from the CriGri-PICRH-1.0 genome assembly. Label (B) represents



the contig assembled from the RGEN long-read sequencing method, aligned to chromosome 3. Label (C) indicates reads aligning to the CHO genome assembly in which the mate in the pair aligned to the expression vector. (C) Estimated copy number per reference genome of the NISTCHO expression vector, reported from the light chain sequence (black bar), heavy chain sequence (gray bar), kanamycin marker in the bacterial backbone (black hatched bar), or glutamine synthetase gene derived from the expression vector (gray hatched bar). All copy numbers are reported relative to the single-copy reference gene *Slc35a1*. (D) PCR amplification across the transgene-vector junction on both the 5' and 3' end of the transgene integration site, as schematically outlined at the top of the panel. Expected amplicon sizes calculated from the assembled contig are noted in red. (E) Droplet digital PCR quantification of the transgene-vector junctions. The ratio of the transgene-vector junction is reported relative to a single-copy gene (*Slc35a1*, black bar) or known three-copy gene (*Fbxw2*, gray hatched bar). Error bars represent the 95% confidence interval of the copy number ratio, as reported by the BioRad QuantaSoft software.

case, a heterotetrameric IgG. Low-molecular weight fragments of the antibody were not observed above the limit of detection, and the presence of 3.2% high-molecular weight aggregates is similar to the 3.0% reported for RM 8671 NISTmAb [18] [Figure 3A].

The NISTmAb IgG, like most recombinant monoclonal antibodies, contains an N-linked glycan on the Fc region [18, 19]. N-glycan profiles can be influenced by the parental cell line, clone-specific factors, and cell culture conditions [20]; therefore, we quantified the relative proportions of the most abundant N-glycan forms as an initial screening assessment. The relative glycoform distributions of cNISTmAb-MPSG and RM 8671 NISTmAb were quantified by mass spectrometry, and the assignment of glycoforms was performed using the intact mass of the IgG heavy chain peptide modified by a single monosaccharide (refer to Supplemental File 1 and Figure S12A for further details on N-glycan species evaluated). Compared to RM 8671 NISTmAb, cNISTmAb-MPSG produced by clone 31 showed a higher relative abundance of G0F (70% vs. 41%) and lower abundances of G1F (20% vs. 43.9%) and G2F glycans (1.5% vs. 11.9%) (Figure 3B). High-

mannose species (Man5) were not detected in cNISTmAb-MPSG produced by clone 31.

The charge profiles of monoclonal antibodies can be influenced by a variety of posttranslational changes [21, 22]. A similar screening assessment was performed using imaged capillary isoelectric focusing (iCIEF) to assess the charge heterogeneity and isoelectric points of the cNISTmAb-MPSG relative to RM 8671 NISTmAb. Acidic, dominant, and basic peaks were assigned as described in Figure 3C, and as expected the dominant peak for RM 8671 NISTmAb is observed at an isoelectric point similar to that reported for the reference material [18] ( $pI \approx 9.2$ ) (Supplemental File 1 and Figure S13). The analysis of RM 8671 NISTmAb demonstrated similar relative fractions of acidic and basic species as what has been previously reported, with approximately 74% of the charge variants being assigned to the dominant peak, 10% to the basic peaks, and 16% assigned to the acidic peaks [18]. For the cNISTmAb-MPSG produced by clone 31, charge variant species were identified at the same isoelectric points as for RM 8671 NISTmAb (Supplemental File 1 and Figure S13), but the

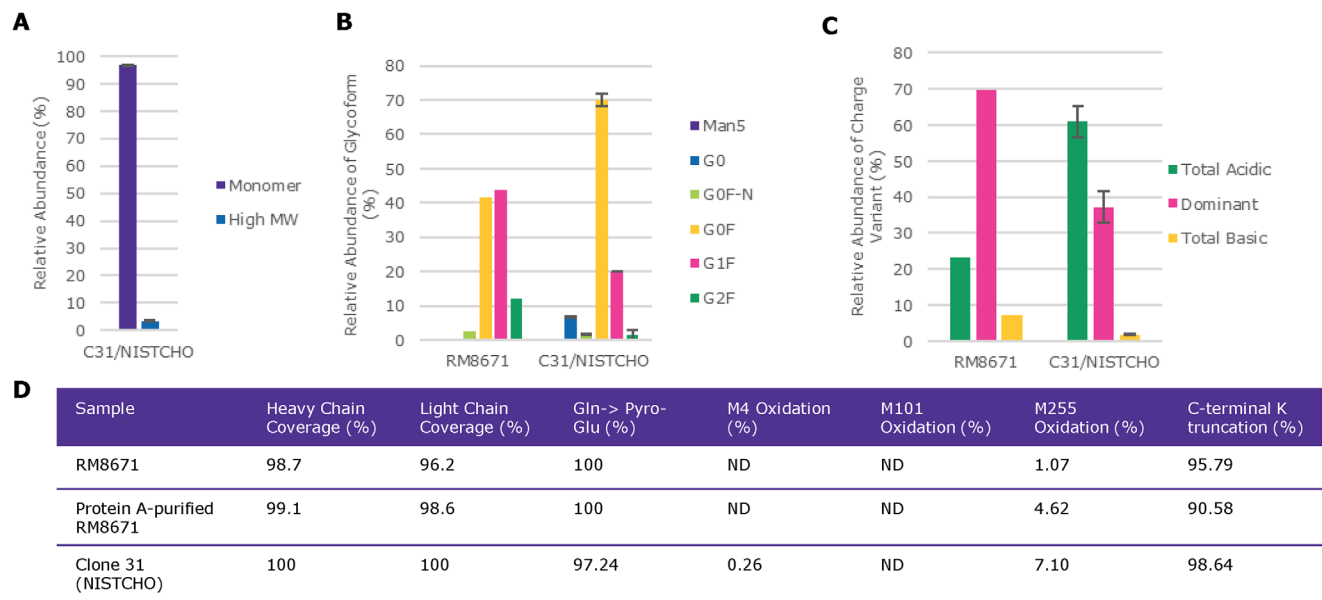


**FIGURE 3** | Product quality attributes meet all selection criteria for cNISTmAb-MPSG produced by NISTCHO in a spin tube cell culture model. In Figures (A)–(C), data are reported as the average of duplicate samples with error bars representing one standard deviation. (A) Assessment of cNISTmAb-MPSG aggregation levels in material produced by NISTCHO. (B) Relative abundance of N-glycan forms, reported as percentage of the total quantified. Rare glycoforms with expected abundance < 1% were not quantified or reported. (C) Relative abundance of charge variant species in cNISTmAb-MPSG produced by NISTCHO in comparison to RM 8671 NISTmAb. The pI of the dominant peak for RM 8671 NISTmAb was used for assignment of acidic, dominant, and basic peaks in all cNISTmAb-MPSG material evaluated. (D) Quantitative assessment of peptide coverage and posttranslational modification performed by LC-MS/MS.

relative abundance of acidic species is greater than for RM 8671 NISTmAb, with 61% of the charged species demonstrating a  $pI < 9.2$  (Figure 3C).

Lastly, we subjected protein A-purified cNISTmAb-MPSG from clone 31 to a tryptic digestion and evaluated the resulting peptides by liquid chromatography tandem mass spectrometry. RM 8671 NISTmAb was analyzed in parallel, including after a parallel protein A purification to assess process-induced artifacts. As described in Figure 3D, high levels of peptide coverage across both the heavy chain and light chain were detected for all samples, with 100% of the expected peptides detected for cNISTmAb-MPSG from clone 31. Expected peptide modifications for a CHO-based process, including conversion of the N-terminal glutamine to pyroglutamic acid and truncation of the C-terminal lysine, were detected in 97% and 98% of the peptides from cNISTmAb-MPSG from clone 31 (Figure 3D). Peptide deamidation was not detected, but low levels of peptide oxidation were detected, primarily at methionine M255 (Figure 3D). As a significant increase in M255 oxidation was observed after protein A purification of RM 8671 NISTmAb, some amount of oxidation can be attributed to the purification process.

## 2.5 | NISTCHO Performance Can Be Validated in an Independent Laboratory

Reference materials benefit from both robust performance of the materials and clearly defined methods for their characterization. To assess these factors, we partnered with the National Institute for Innovation in Manufacturing Biopharmaceuticals (NIIMBL) for technology transfer and validation of the fed-batch production process established previously in a spin tube culture model. In this study, we evaluated clone 31 in bioreactor systems commonly used for cell line and process development, including the Ambr 15 and Ambr 250 (Sartorius) microbioreactor platforms at Site 1 and Site 2, respectively. The initial bioreactor process conditions, described in detail in the Materials and Methods, were established based on the recommendations provided in the CHOZN GS<sup>-/-</sup> Platform Technical Bulletin [22], and the inoculation and alternative feeding strategies were maintained from the previous studies described for Figure 1E–G.

Compared to the previous assessment in a spin tube model, clone 31 demonstrated similar peak viable cell density but slightly improved culture viability through assay day 15 when operated in these small-scale bioreactor models (Figure 4A). The overall growth patterns and viability profiles were similar, and peak viable cell density differed by 11% ( $2.7 \times 10^6$  cells/mL) between sites. Compared to the spin tube model, a slight improvement in peak volumetric titer was observed at both sites, with peak volumetric titers reaching 3.0 (Site 1) and 2.4 g/L (Site 2) (Figure 4B); peak volumetric titer differed by 20% (0.6 g/L) for site 2 compared to site 1. Lastly, the metabolite profiles were also evaluated in these cultures to assess the suitability of clone 31 for further study. All cultures at both sites demonstrated appropriate maintenance of glucose levels with the feeding strategy applied (Figure 4C). In alignment with the feeding strategy, an accumulation of lactate in the early stages of the process was observed, with peak lactate levels remaining near or below 2 g/L and dropping rapidly after day 7, indicating an expected shift from lactate production to

lactate consumption (Figure 4C). Ammonium levels were maintained at modest levels throughout the duration of the experiment and were comparable between sites (Figure 4D), with only slight differences observed on days 9 and 14 or 15. Similar metabolite profiles were observed for glutamine, glutamate, potassium, and calcium between sites (Figures 4D–E).

## 3 | Discussion

In this work, we describe the foundational studies to develop and characterize the first reference cell line to be distributed by NIST, which serves as the US National Metrology Institute. To provide accessible experimental reagents to scientists worldwide and enable NIST to establish this cell line as a reference standard, we provide an unprecedented level of detail into the cell line development and characterization process. In this discussion, we provide further insight into how the NISTCHO cell line was selected for further development (Figure 5).

The initial candidate selection sought to identify a cell line producing a minimum volumetric titer of 2 g/L in an unoptimized fed-batch assay using commercially available cell culture medium and feeds, a target which was exceeded for all candidates. Maintenance of volumetric productivity after extended passage is a clear expectation in biotherapeutic manufacturing, and here we expected the cell line should maintain > 70% of the volumetric titer of the RCB after at least 60 population doublings. All six candidates surpassed this threshold using the improved feeding strategy, although one clone did not achieve this benchmark in the original process.

The second set of criteria relating to the transgene integration site proved to be the most impactful in the selection of the NISTCHO cell line. It must be possible to confirm the identity of the NISTCHO cell line unambiguously with tractable, accessible methods. The clonal cell line must possess mappable, unique chromosomal breakpoints at the 5' and 3' end of the integrated vector, and the integration site must not be duplicated with other clones assessed in the project. In addition, we preferred to have clones possessing 2–5 copies of the transgene, a range that is representative of many cell lines developed using the CHOZN GS<sup>-/-</sup> platform. Clones 2 and 6 were disqualified due to their shared integration site, as they could not be reliably distinguished from one another at this locus. The transgene integration site for clone 21 contained sequences that were not mappable to the CHO genome, disqualifying this clonal cell line for further consideration. While clones 13, 15, and 31 all met the criteria to establish a PCR-based assay for cell line identification, clone 31 was selected for further development as NISTCHO due to its alignment with industry-representative transgene copy numbers. This selection was finalized after the transgene integration site was further verified using short read-sequencing and PCR methods.

Third, we evaluated a variety of product quality attributes for the cNISTmAb-MPSG produced by these candidate cell lines. The primary objective was to exclude any clonal cell line producing material with problematic characteristics, specifically high aggregate or LMW fragment levels, elevated levels of high mannose N-glycans, or high levels of charge variant species that are not

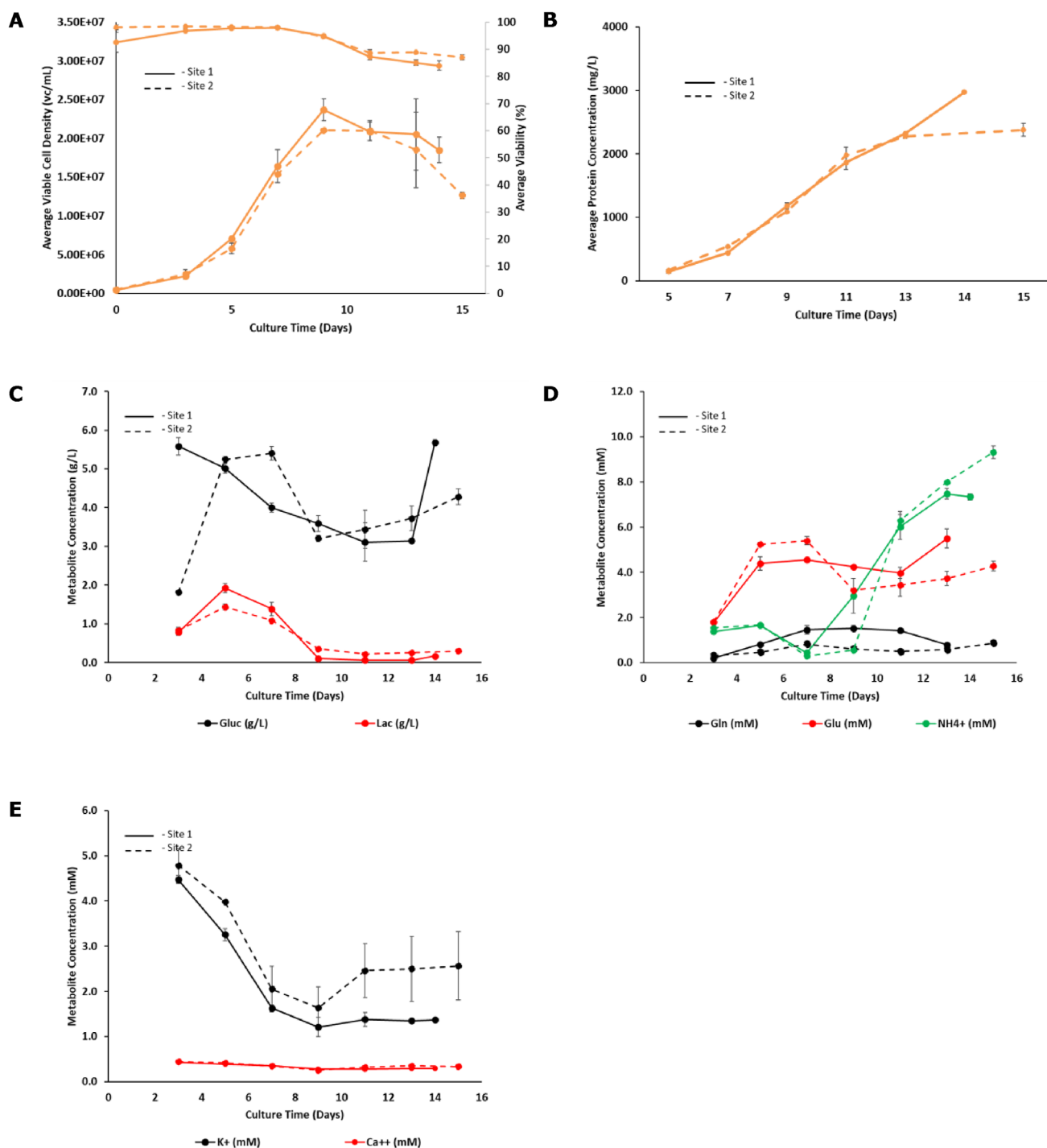


**FIGURE 4** | Performance comparability of NISTCHO using a bioreactor cell culture model is satisfactory during an interlaboratory study. Data are reported as the average of duplicate samples with error bars representing one standard deviation. In all panels, solid line indicates site 1 (Ambr 15) and dotted line indicates site 2 (Ambr 250). (A) Growth and viability profiles for NISTCHO. (B) Product titer profile for cNISTmAb-MPSG or cNISTmAb-NMBL produced by NISTCHO. (C) Metabolite profiles for glucose (black) and lactate (red) in NISTCHO cultures. (D) Metabolite profiles for glutamine (black), glutamate (red), and ammonium (green). (E) Metabolite profiles for potassium (black) and calcium (red).

present in RM 8671 NISTmAb. It was also desired that the cNISTmAb-MPSG produced by the NISTCHO reference cell line should have different product quality attributes compared to RM 8671 NISTmAb, which would further enable evaluation of new methods and equipment using material with different properties. Importantly, while it is known that RM 8671 NISTmAb was produced in the mammalian NS0 cell line, no details regarding

the upstream or downstream processes are publicly available for this material. It is reasonable to expect product quality differences when a recombinant protein is expressed in different host cell lines, but due to these information limitations it is not possible to assess the root cause of product quality differences between RM 8671 NISTmAb and cNISTmAb-MPSG. The cNISTmAb-MPSG produced by all candidate cell lines met all selection criteria,



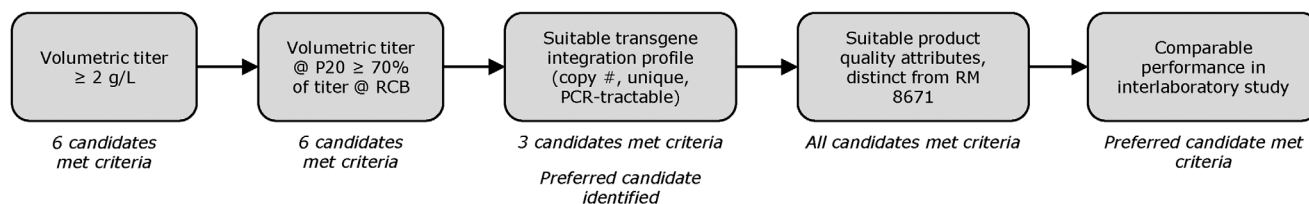


**FIGURE 5** | The NISTCHO reference cell line was selected based on predetermined criteria. This decision tree reports how candidates were evaluated based on volumetric titer, stability of recombinant protein expression, transgene integration profile, recombinant product quality attributes, and performance in an interlaboratory study.

displaying acceptable product quality attributes with different relative abundances compared to RM 8671 NISTmAb.

As a final confirmation of the suitability of clone 31 for distribution as a future reference material, we performed a comparability assessment using small-scale bioreactor technologies at the original site and at an independent laboratory. Importantly, the overall growth, productivity, and metabolic trends for these cell lines were maintained between the two sites. With the successful completion of these technology transfer exercises, we have completed the initial characterization and selection of the NISTCHO cell line. Additional insights around the genetic and performance attributes and optimal process conditions will continue to be developed through collaborative, interlaboratory studies organized by NIST and performed by the scientific community.

## 4 | Materials and Methods

### 4.1 | Product Nomenclature and Definitions

To describe the recombinant protein produced, the following naming conventions were applied in alignment with the existing NIST naming conventions. The prefix “c” in cNISTmAb designates nonoriginator material, produced in CHO cell lines, that shares the same mature protein sequence as NISTmAb. Only reference material distributed by NIST will leverage this nomenclature with no suffix. A suffix is then defined based on draft FDA guidance for biosimilar naming [23] which would thus utilize a form of “cNISTmAb-YYYY,” where YYYY is a company or institution-specific four letter identifier. In this manuscript, cNISTmAb-MPSG or cNISTmAb-NMBL identifiers are utilized to describe recombinant protein produced by any of the cell lines under consideration, and when required, clone-specific products can be communicated through clonal identifiers. Additional guidance on cell line and recombinant protein nomenclature can be found on the NISTCHO product page (<https://www.nist.gov/programs-projects/nistcho>) and as published by Cleveland, et al. [24].

### 4.2 | Generation of Clonal Cell Lines

The following protocols were leveraged for clonal cell line development and are based on existing published protocols [25]. To develop the expression vector used to generate the NISTCHO cell line, first, the mature IgG1 sequences for NISTmAb [26] were used to query the NCBI nonredundant protein database [27].

Signal peptide sequences were identified from peptide sequences for full-length antibodies sharing homology with the N-terminal fragment of the heavy and light chains of NISTmAb. A complete description of the cell line development process is included in Supplemental File 1.

### 4.3 | Growth and Productivity Assessments in Spin Tube and Bioreactor Models

Frozen vials of cells were thawed and cultivated in EX-CELL CD CHO Fusion without L-glutamine as described in Supplemental File 1. After 2–3 passages, cultures were inoculated at an initial density of  $0.3 \times 10^6$  cells/mL in EX-CELL Advanced CHO Fed-Batch basal medium (MilliporeSigma, cat. 24365C). In the initial screening fed-batch assay, EX-CELL Advanced CHO Feed 1 (MilliporeSigma, cat. 24366C) was prepared according to the manufacturer’s instructions and sterilized using a 0.2  $\mu$ m filter (MilliporeSigma, cat. SCGPU10RE). In this assay, starting on day 3 postinoculation and every other day through the remainder of the assay, cultures were supplemented with 5% v/v of the feed and glucose was supplemented to a final concentration of 6 g/L using a sterile glucose solution (MilliporeSigma, cat. G8769). EX-CELL Advanced CHO Feed 1 (MilliporeSigma, cat. 24366C) and Cellvento 4Feed (MilliporeSigma, cat. 103796) were prepared separately according to the manufacturer’s instructions, and a mixture of 67% v/v EX-CELL Advanced CHO Feed 1 and 33% v/v Cellvento 4Feed was prepared and sterilized using a 0.2  $\mu$ m filter (MilliporeSigma, cat. SCGPU10RE). Starting on day 3 postinoculation and every other day through the remainder of the assay, cultures were supplemented with 5% v/v of the blended feed and glucose was supplemented to a final concentration of 8 g/L using a sterile glucose solution (MilliporeSigma, cat. G8769). The assays were continued until the culture reached  $\leq 70\%$  viability or until day 21 (spin tube models) or day 14 (bioreactors). Starting on day 3 postinoculation and every other day through the remainder of the assay, culture samples were collected for cell density and viability measurements (Vi-CELL XR, Beckman Coulter) or for protein titer or product quality measurements, which utilize samples clarified by centrifugation at 500 x g. Metabolite measurements were performed using a BioProfile FLEX2 (Nova Biomedical) using clarified supernatants.

The Ambr 15 (Site 1) and Ambr 250 (Site 2) small-scale bioreactor systems (Sartorius) were utilized for all bioreactor experiments described and were performed as follows. Prior to inoculation, Ambr 15 vessels were filled with 10 mL of EX-CELL Advanced CHO Fed-batch medium and dissolved oxygen was calibrated overnight at 100% air saturation with temperature control at 37°C.

All vessels were inoculated at a targeted viable cell density of  $0.5 \times 10^6$  cells/mL. All pH calibrations were performed utilizing the Ambr analysis module. The pH set point  $6.9 \pm 0.05$  was maintained with additions of 7.5% sodium carbonate solution (MilliporeSigma, cat. 223530), or by sparging  $\text{CO}_2$ . Agitation rate was set to 950RPM (Ambr 15) or 300 RPM (Ambr 250), and the dissolved oxygen (DO) was set to 40%.

Measurement of protein titer or product quality attributes are described in Supplemental File 1 and utilized clarified supernatants. Methods relating to genetic characterization, including sequencing and PCR, are described in detail in Supplemental File 1.

## Author Contributions

Hussain Dahodwala, Irfan Hodzic, Alexei Slesarev, Alexander Kuzin, Rahul Lal, Jiajian Liu, James Mahon, Rajagopalan Lakshmi Narasimhan, Jaya Onuska, James Ravellette, Kelsey Reger, Sadie Sakurada, and Floy Stewart performed experiments, analyzed results, and wrote the manuscript. Benjamin Cutak analyzed results, designed experiments, and wrote the manuscript. Trissa Borgschulte, Colette Cote, Kelvin Lee, William O'Dell, and Zvi Kelman designed experiments, interpreted results, and revised the manuscript. Britta Anderson designed experiments, analyzed and interpreted results, and wrote the paper.

## Acknowledgments

The authors wish to thank the following colleagues for their support for this manuscript: Joe Orlando and Kimberly Mann for signal peptide screening; Daniel Miller for cell culture tasks; Christine Caseres, Felicia Riordan, Ken Chantramontri, Carolyn Cash, and Scott Wilson for analytical experiment tasks; and Jason Gustin, Amber Petersen, and David Razafsky for critical feedback on this manuscript. H.D. and K.H.L. would like to acknowledge support from the Department of Commerce NIST through 70NANB17H002.

## Conflicts of Interest

The authors declare no conflicts of interest.

## Data Availability Statement

The annotated plasmid sequence for the expression vector used in these studies has been deposited within GenBank under accession number PP445015. An annotated contig describing the transgene integration site for clone 31, inclusive of chromosomal flanking sequences, has been deposited within GenBank under accession number PP565930. Nanopore sequencing data for all six candidate cell lines and Illumina sequencing data for clone 31 have been deposited in the Sequence Read Archives under BioProject PRJNA1082661. Data from NISTCHO is provided in Excel format in Supplemental File 4 (NISTCHO Data). Details regarding access to the NISTCHO cell line are available on the NISTCHO product page (<https://www.nist.gov/programs-projects/nistcho>) or by contacting [nistcho@nist.gov](mailto:nistcho@nist.gov).

## References

1. National Institute of Standards and Technology. *Metrological Traceability Frequently Asked Questions and NIST Policy*. (U.S. Department of Commerce, 2021), <https://www.nist.gov/publications/metrological-traceability-frequently-asked-questions-and-nist-policy>.
2. National Institute of Standards and Technology. *NIST Monoclonal Antibody Reference Material 8671|NIST* (U.S. Department of Commerce, 2023), <https://www.nist.gov/programs-projects/nist-monoclonal-antibody-reference-material-8671>.

3. C. T. Korch, E. M. Hall, W. G. Dirks, et al., *Human Cell Line Authentication: Standardization of Short Tandem Repeat (STR) Profiling* (ATCC Standards Development Organization, 2021), <https://webstore.ansi.org/standards/atcc/ansiatccasn00022022>.
4. J. L. Almeida and C. T. Korch (2023) "Authentication of Human and Mouse Cell Lines By Short Tandem Repeat (STR) DNA Genotype Analysis," in ed. *Assay Guidance Manual*, S. Markossian, A. Grossman, M. Arkin, D. Auld, C. Austin, J. Baell, K. Brimacombe, T.D.Y. Chung, et al. (Eli Lilly & Company and the National Center for Advancing Translational Sciences, 2023), <https://www.ncbi.nlm.nih.gov/books/NBK144066/>.
5. National Institute of Standards and Technology. *NISTCHO Test Material Guidance Document* (U.S. Department of Commerce, 2023), <https://tsapps.nist.gov/srmext/certificates/10197.pdf>.
6. F. V. Ritacco, Y. Wu, and A. Khetan, "Cell Culture media for Recombinant Protein Expression in Chinese Hamster Ovary (CHO) Cells: History, Key Components, and Optimization Strategies," *Biotechnology Progress* 34, no. 6 (2018): 1407–1426, <https://doi.org/10.1002/btpr.2706>.
7. J. Ehret, M. Zimmermann, T. Eichhorn, and A. Zimmer, "Impact of Cell Culture Media Additives on IgG Glycosylation Produced in Chinese Hamster Ovary Cells," *Biotechnology and Bioengineering* 116, no. 4 (2019): 816–830, <https://doi.org/10.1002/bit.26904>.
8. J. Kaiser and M. Brandl, *Improving Fed-Batch Yields By Combining EX-CELL® Advanced and Cellvento® Cell Culture Media Portfolios* (MilliporeSigma, 2022), <https://www.sigmaldrich.com/deepweb/assets/sigmaldrich/marketing/global/documents/343/115/improving-fed-batch-yields-wp8492en-ms.pdf>.
9. H. Dahodwala and K. H. Lee, "The Fickle CHO: A Review of the Causes, Implications, and Potential Alleviation of the CHO Cell Line Instability Problem," *Current Opinion in Biotechnology* 60 (2019): 128–137, <https://doi.org/10.1016/j.copbio.2019.01.011>.
10. J. L. Almeida, K. D. Cole, and A. L. Plant, "Standards for Cell Line Authentication and Beyond," *PLoS Biology* 14, no. 6 (2016): 1002476, <https://doi.org/10.1371/journal.pbio.1002476>.
11. A. Slesarev, L. Viswanathan, Y. Tang, et al., "CRISPR/CAS9 Targeted CAPTURE of Mammalian Genomic Regions for Characterization by NGS," *Scientific Reports* 9, no. 1 (2019): 3587, <https://doi.org/10.1038/s41598-019-39667-4>.
12. A. Kuzin, B. Redler, J. Onuska, and A. Slesarev, "RGEN-Seq for Highly Sensitive Amplification-Free Screen of Off-Target Sites of Gene Editors," *Scientific Reports* 11, no. 1 (2021): 23600, <https://doi.org/10.1038/s41598-021-03160-8>.
13. O. Rupp, M. L. MacDonald, S. Li, et al., "A Reference Genome of the Chinese Hamster Based on a Hybrid Assembly Strategy," *Biotechnology and Bioengineering* 115, no. 8 (2018): 2087–2100, <https://doi.org/10.1002/bit.26722>.
14. C. S. Kaas, C. Kristensen, M. J. Betenbaugh, and M. R. Andersen, "Sequencing the CHO DXB11 Genome Reveals Regional Variations in Genomic Stability and Haploidy," *BMC Genomics* 16, no. 1 (2015): 160, <https://doi.org/10.1186/s12864-015-1391-x>.
15. C. Kretzmer, R. L. Narasimhan, R. D. Lal, et al., "De Novo Assembly and Annotation of the CHOZN® GS –/– Genome Supports High-Throughput Genome-Scale Screening," *Biotechnology and Bioengineering* 119, no. 12 (2022): 3632–3646, <https://doi.org/10.1002/bit.28226>.
16. L. K. Hmiel, K. A. Brorson, and M. T. Boyne, "Post-Translational Structural Modifications of Immunoglobulin g and Their Effect on Biological Activity," *Analytical and Bioanalytical Chemistry* 407, no. 1 (2015): 79–94, <https://doi.org/10.1007/s00216-014-8108-x>.
17. Y. Lu, L. A. Khawli, S. Purushothama, F. P. Theil, and M. A. Partridge, "Recent Advances in Assessing Immunogenicity of Therapeutic Proteins: Impact on Biotherapeutic Development," *Journal of Immunology Research* 2016 (2016): 8141269, <https://doi.org/10.1155/2016/8141269>.

18. K. Yandrowski, J. E. Schiel, T. Mouchahoir, et al., *Humanized Monoclonal Antibody IgG1k, NISTmAb RM 8671 Summary of 5 Year Stability Verification (5YSV)* (National Institute of Standards and Technology Special Publication (SP) NIST SP 260-237, 2023), <https://doi.org/10.6028/NIST.SP.260-237>.
19. M. L. A. De Leoz, D. L. Duewer, A. Fung, et al., “NIST Interlaboratory Study on Glycosylation Analysis of Monoclonal Antibodies: Comparison of Results From Diverse Analytical Methods,” *Molecular and Cellular Proteomics* 19, no. 1 (2020): 11–30, <https://doi.org/10.1074/mcp.ra119.001677>.
20. E. Edwards, M. Livanos, A. Krueger, et al., “Strategies to Control Therapeutic Antibody Glycosylation During Bioprocessing: Synthesis and Separation,” *Biotechnology and Bioengineering* 119, no. 6 (2022): 1343–1358, <https://doi.org/10.1002/bit.28066>.
21. A. Beck, C. Nowak, D. Meshulam, et al., “Risk-Based Control Strategies of Recombinant Monoclonal Antibody Charge Variants,” *Antibodies* 11, no. 4 (2022): 73, <https://doi.org/10.3390/antib11040073>.
22. F. Füssl, K. Cook, K. Scheffler, A. Farrell, S. Mittermayr, and J. Bones, “Charge Variant Analysis of Monoclonal Antibodies Using Direct Coupled pH Gradient Cation Exchange Chromatography to High-Resolution Native Mass Spectrometry,” *Analytical Chemistry* 90, no. 7 (2018): 4669–4676, <https://doi.org/10.1021/acs.analchem.7b05241>.
23. Food and Drug Administration. *Nonproprietary Naming of Biological Products: Update. Guidance for Industry* (U.S. Department of Health and Human Services, 2019), <https://www.fda.gov/media/121316/download>.
24. M. H. Cleveland, I. L. Karageorgos, J. P. Marino, et al., “Recommended Nomenclature Convention for the NISTCHO Cell Line and its Product Monoclonal Antibody, CNISTmAb,” *mAbs* (accepted for publication).
25. MilliporeSigma. *CHOZN Platform Technical Bulletin* (MilliporeSigma, 2011), <https://www.sigmaaldrich.com/deepweb/assets/sigmaaldrich/product/documents/245/459/chozn-platform-technical-bulletin.pdf>.
26. National Institute of Standards and Technology. *Reference Material® 8671 NISTmAb, Humanized IgG1k Monoclonal Antibody* (U.S. Department of Commerce, 2022), <https://tsapps.nist.gov/srmext/certificates/8671.pdf>.
27. N. A. O’Leary, M. W. Wright, J. R. Brister, et al., “Reference Sequence (RefSeq) Database at NCBI: Current Status, Taxonomic Expansion, and Functional Annotation,” *Nucleic Acids Research* 44, no. D1 (2016): D733–D745, <https://doi.org/10.1093/nar/gkv1189>.

### Supporting Information

Additional supporting information can be found online in the Supporting Information section.